Imaging neural activity in worms, flies and mice with improved GCaMP calcium indicators

Lin Tian[1], S. Andrew Hires[1], Tianyi Mao[1], Daniel Huber[1], M. Eugenia Chiappe[1], Sreekanth H. Chalasani[2], Leopoldo Petreanu[1], Jasper Akerboom[1], Sean A. McKinney[1,3], Eric R. Schreiter[4], Cornelia I. Bargmann[2], Vivek Jayaraman[1], Karel Svoboda[1], Loren L. Looger[1†]

[1] Howard Hughes Medical Institute, Janelia Farm Research Campus, Ashburn, VA 20147, USA
[2] Howard Hughes Medical Institute, Laboratory of Neural Circuits and Behavior, The Rockefeller University, New York, NY 10065, USA
[3] Current address: The Stowers Institute, Kansas City, MO 64110, USA
[4] Department of Chemistry, University of Puerto Rico – Río Piedras, San Juan, Puerto Rico 00931

[†]Correspondence should be addressed to L. L. L. (loogerl@janelia.hhmi.org)

ABSTRACT

Genetically encoded calcium indicators (GECIs) can be used to image activity in defined neuronal populations. However, current GECIs produce inferior signals compared to synthetic indicators and recording electrodes, precluding detection of low firing rates. We developed a single-wavelength GECI based on GCaMP2 (GCaMP3), with increased baseline fluorescence (3x), dynamic range (3x), and higher affinity for calcium (1.3x). GCaMP3 fluorescence changes triggered by single action potentials were detected in pyramidal cell dendrites, with signal-to-noise ratio and photostability significantly better than GCaMP2, D3cpVenus, and TN-XXL. In *Caenorhabditis* chemosensory neurons and the *Drosophila* antennal lobe, sensory stimulation-evoked fluorescence responses were significantly enhanced with the new indicator (4-6x). In somatosensory and motor cortical neurons in the intact mouse, GCaMP3 detected calcium transients with amplitudes linearly dependent on action potential number. Long-term imaging in the motor cortex of behaving mice revealed large fluorescence changes in imaged neurons over months.

INTRODUCTION

Calcium is a universal second messenger regulating essential cellular signaling events in a broad range of tissues and organisms. In neurons, action potentials (APs) trigger large and rapid changes in cytoplasmic free calcium. Similarly, activation of synaptic glutamate receptors during synaptic transmission produces [Ca^{2+}] transients in dendritic spines. Calcium imaging using synthetic calcium indicators has been used to measure neuronal spiking and synaptic input across populations of neurons *in vitro* [1] and *in vivo* [2,3]. However, synthetic indicators are difficult to target to specific cell types or sub-cellular locations (but see [4]). The loading procedures are invasive and damaging to neural tissue, precluding repeated, chronic *in vivo* measurements.

Genetically encoded calcium indicators (GECIs) (also called fluorescent calcium indicator proteins; FCIPs) provide an alternative to synthetic indicators. GECIs can be easily targeted to specific cell types or sub-cellular compartments (for review see [5]). They are compatible with long-term, repeated *in vivo* measurements [6]. GECIs consist of a calcium-binding domain such as calmodulin or troponin C, fused to either one or two fluorescent proteins (FPs) (for review see [7,8]). In single-FP GECIs, the fluorescence intensity of a circularly permuted FP (cpFP) is modulated by calcium binding-dependent changes in the chromophore environment [9,10]. In two-FP GECIs, calcium binding modulates fluorescence resonance energy transfer (FRET) between FPs [11-13].

GECIs have been iteratively improved, and are becoming useful for quantitative imaging of neural activity *in vivo*. The calmodulin-based FRET indicator D3cpVenus (D3cpV) [13] has recently been reported to detect single APs in pyramidal neurons in organotypic mouse brain slices and *in vivo* [14]. The troponin C-based indicator TN-XXL has been used for chronic *in vivo*

activity imaging in the mouse brain [6]. Among single-FP based GECIs, the GCaMP family has found the broadest use across multiple model organisms [15-17]. However, the properties of all available GECIs are still inferior to synthetic indicators in terms of signal-to-noise ratio (SNR), response linearity, photostability, and properly tuned calcium affinity. The GCaMP indicators further suffer from poor protein stability. Improvements in each of these parameters would facilitate imaging of neural activity.

Recently, the Ca^{2+}-bound and -free structures of GCaMP2 have been solved [18,19], forming the basis for rational improvement of indicator properties. Using a combination of protein structure-guided mutagenesis and semi-rational library screening (for review of GECI design, see [20]), we developed improved GCaMP variants. The best mutant, GCaMP3, is brighter, possesses greater protein stability, and has a larger dynamic range and higher affinity for calcium compared to GCaMP2. GCaMP3 is more photostable than the FRET indicators D3cpV and TN-XXL and displays significantly greater sensitivity and faster kinetics, especially at higher levels of activity. GCaMP3 showed improved sensitivity in mammalian cell culture, pyramidal neurons in brain slices, and worms, flies, and mice *in vivo*.

RESULTS

Structure-guided engineering of GCaMP3

In HEK293 cells the fluorescence of GCaMP2 is one hundred fold lower than EGFP (**Supplementary Fig. 1a**). Addition of a proteasome inhibitor (10 μM lactacystin) increased the baseline fluorescence of HEK293 cells expressing GCaMP2 (**Supplementary Fig. 1b**). We reasoned that an N-terminal arginine, found immediately after the initiator methionine of GCaMP2, might destabilize the protein [21]. Indeed, HEK293 cells transfected with a mutant lacking the arginine, named GCaMP2.1, showed 40% higher baseline fluorescence than those transfected with GCaMP2 (**Supplementary Fig. 1b**).

We then created small libraries of GCaMP2.1 variants *via* site-directed mutagenesis at many sites, both near the EGFP chromophore and at "superfolder GFP" positions [22] (**Supplementary Fig. 2**). Although screening of GCaMP mutants in bacterial lysate achieved high throughput, we found that the baseline fluorescence and dynamic range correlated only weakly with more intact preparations (**Supplementary Fig. 3**). Therefore, we designed a medium-throughput mammalian cell-based assay in HEK293 cells. Calcium transients were induced by activating endogenous muscarinic receptors with acetylcholine (**Supplementary Fig. 3d**). Acetylcholine titrations of GCaMP-transfected HEK293 cells revealed two point mutants with increased dynamic range and baseline fluorescence (T116V; GFP T203V and M66K; GFP M153K). One single (T116V) mutant and a double mutant (T116V and M66K) were named GCaMP2.2, GCaMP2.3, respectively (**Fig. 1a, Supplementary Fig. 4 and Supplementary Table 1**).

To increase GCaMP's affinity for calcium to allow better detection of the small and rapid calcium increases associated with individual APs, we analyzed mutations in the EF-hands and

the interface between the M13 peptide and calmodulin (CaM) (**Supplementary Fig. 2**). The amino acid substitution N363D (CaM N60D) to both GCaMP2.2 and GCaMP2.3 increased the fluorescence change for small calcium transients, with little effect on baseline fluorescence (**Fig. 1a and Supplementary Fig. 4**). GCaMP2.2-N363D and GCaMP2.3-N363D were named GCaMP2.4 and GCaMP3, respectively (**Fig. 1a,b and Supplementary Table 1**). GCaMP3 showed the largest signal change in the acetylcholine assay (**Fig. 1a,b and Supplementary Fig. 4**) and was further characterized.

The fluorescence spectra of purified GCaMP3 are similar to those of GCaMP2, with a slight red-shifting of the excitation maximum (**Fig. 1c**). GCaMP3 protein assayed in 3-(N-morpolino)propanesulfonic acid (MOPS) buffer had a dynamic range (F_{max}/F_{min}) of ~12, 3-fold larger than GCaMP2 (**Fig. 1d-inset**). This results from a 2-fold decrease of calcium-free fluorescence and a 1.5-fold increase of calcium-saturated fluorescence (**Fig. 1c-inset**). The affinity of GCaMP3 for Ca^{2+} was ~1.3-fold higher than GCaMP2 (660 ±19 nM versus 840 ± 25 nM, (p = 0.0017, paired t-test)) (**Fig.1d**).

In HEK293 cells GCaMP3 showed ~2.6-fold higher baseline fluorescence than GCaMP2 (**Fig. 1e- top**). When expressed *via* viral gene transduction in cortical layer 2/3 neurons, baseline fluorescence was ~3.9-fold higher than GCaMP2 (**Fig. 1e- bottom**). Given the lower fluorescence of purified GCaMP3 in the apo state, the increase in baseline fluorescence is likely caused by increased protein expression and stability at 37^{o}C.

Characterization of GCaMP3 in brain slice

We measured the AP-triggered fluorescence responses of GCaMP3 in pyramidal neurons in cultured brain slices (**Fig. 2a,b**) [23,24] and acute neocortical brain slices at room temperature (**Fig. 2c,d**). In cultured slice, GCaMP3 was delivered by biolistic transfection. Increases in GCaMP3 fluorescence intensity ($\Delta F/F=46 \pm 4.2\%$, $n = 9$ cells) at the base of the apical dendrite were detected reliably in response to single APs in all cells (100% single-trial detection; **Supplementary Fig. 5a**). The average $\Delta F/F$ of GCaMP3 ($n = 9$ cells) was 185 ± 13%, 250 ± 27%, 320 ± 35%, 480 ± 50%, 600 ± 100%, and 620 ± 130% for 2, 3, 5, 10, 20 and 40 AP, respectively (**Fig. 2b,e**). The signal-to-noise ratio (SNR; see **Methods**) of GCaMP3 was 16.3 ± 10.9, 167.1 ± 65.1 and 371.4 ± 102.8 for 1 AP, 5 AP and 40 AP, respectively (**Fig. 2f**). The fluorescence increase and single AP detection efficiency are significantly improved over GCaMP2 (1 AP $\Delta F/F = 17\pm10\%$; 38% single-trial detection) [24]. The kinetics of GCaMP3 in cultured hippocampal slice are similar to those of GCaMP2 (GCaMP3: rise $T_{1/2} = 83 \pm 2$ ms; decay $T_{1/2}= 610 \pm 32$ ms; GCaMP2: rise $T_{1/2}=95 \pm 15$ ms; decay $T_{1/2}= 480 \pm 130$ ms[24]; all measurements for 10 AP stimulus). The improved properties of GCaMP3 allow imaging spontaneous population activities in cultured hippocampal slice, as opposed to GCaMP2 (**Supplementary Movies 1, 2 and Supplementary Fig. 6**).

We next tested the performance of GCaMP3 in layer 2/3 (L2/3) somatosensory cortical pyramidal neurons following long-term expression driven by the CAG promoter *via in utero* electroporation (**Fig. 2c and Supplementary Fig. 5b**). The average $\Delta F/F$ of GCaMP3 at the base of the apical dendrite was $14\pm2.7\%$ ($n = 9$ cells) for single action potentials, and 505 ± 220% for 40 APs (**Supplementary Fig. 5b, Fig. 2d,g and Supplementary Table 2**). Compared to GCaMP2 ($n = 8$ cells), the $\Delta F/F$ and SNR of GCaMP3 were 2-5 fold larger (**Fig. 2g,h and**

Supplementary Table 2). Individual action potentials in single trials could be resolved at rates up to 6 Hz (**Supplementary Fig. 7**). The threshold for 100% spike detection in acute brain slices was 2 APs, with a 1 AP detection rate of ~90% (**Supplementary Figs. 5b and 8a**), slightly inferior to the performance in cultured brain slices. The source of this discrepancy is unknown.

Comparison of GCaMP3 and FRET-based GECIs

We compared the performance of D3cpV and TN-XXL (**Fig. 3a**) to GCaMP3 under identical experimental conditions. At baseline calcium levels, the FRET indicators (based on intact fluorescent proteins) were brighter than GCaMP3 (data not shown). However, the smaller fluorescence changes produced by the FRET indicators (**Supplementary Fig. 9, Fig. 3b,c and Supplementary Table 2**) resulted in lower SNR compared to GCaMP3 (**Fig. 3d-f and Table 2**). Furthermore, GCaMP3 was more photostable than the FRET indicators. Following 10 cycles of 150 seconds of frame-scan illumination of the soma and proximal dendrite (10 mW at the sample), interspersed by 30 seconds of darkness, GCaMP3 fluorescence remained unchanged (109% of starting fluorescence), whereas TN-XXL (36% CFP; 70% YFP) and D3cpV (59% CFP; 84% YFP) showed reduced fluorescence (**Fig. 3g**). The mean fluorescence rise times were similar: 95 ± 27 ms, 80 ± 18 ms, and 108 ± 26 ms for GCaMP3, TN-XXL and D3cpV (**Fig. 3h-left**). The fluorescence decay time of GCaMP3 (650 ± 230 ms, n = 7 cells), was significantly shorter than for the FRET indicators (TN-XXL, 1550 ± 640 ms, n = 10 cells (p = 0.0016, paired t-test); D3cpV, 9500 ± 3400 ms, n = 10 cells (p = 1.7e-05, paired t-test)) (**Fig. 3h- right**).

In terms of absolute response and SNR, GCaMP3 performed better than both FRET indicators over the entire stimulus range, particularly from 2-20 APs (**Fig. 3f and Table 2**).

GCaMP3 also showed greater photostability and faster kinetics (**Fig. 3g,h**). These factors translate into improved detection and measurement of physiologically relevant calcium signals (**Supplementary Fig. 8a**).

Imaging sensory-evoked Ca^{2+} transients in worms

To compare the performance of GCaMP3 with previous GCaMPs in response to sensory stimulation-evoked activity in sensory neurons, we created stable worm lines expressing GCaMP1, GCaMP2 and GCaMP3 in one of the two AWC neurons (AWC^{ON}). Expression of GCaMP1 and GCaMP2 in AWC neurons caused behavioral perturbations in some of transgenic lines, reflected by decreased local search turning. In contrast, GCaMP3-expressing worms showed no detectable cytotoxicity or behavioral perturbation (**Supplementary Fig. 10 and Supplementary Table 3**). Individual worms were imaged following an odour addition-removal sequence [16]. Presentation of isoamyl alcohol inhibited AWC^{ON}, causing a decrease in fluorescence for all three GCaMP indicators (**Fig. 4a,b**). The fluorescence change was larger for the two newer GCaMPs relative to GCaMP1 (-13 ± 6% for GCaMP1, -27 ± 8% for GCaMP2, -38 ± 8% for GCaMP3). Subsequent removal of the attractive odour resulted in an average of 455 ± 48% fluorescence increase in AWC^{ON} neurons expressing GCaMP3, a ~4-5-fold improvement over GCaMP2 (113 ± 25% $\Delta F/F$) and GCaMP1 (88 ± 19% $\Delta F/F$) (**Fig. 4c,d**). Variation in sensor expression levels due to the mosaic nature of transgenesis precluded quantitative comparison of indicator baseline brightness.

Imaging sensory-evoked Ca^{2+} transients in flies

We then expressed GCaMP1.6 and GCaMP3 in a broad subset of *Drosophila* olfactory projection neurons (PNs) in the antennal lobe (AL) and compared their responses to odour application (GCaMP2 does not express well in *Drosophila* [25]). Single copies of GCaMP were sufficient to produce visible fluorescence (data not shown) in glomeruli of the antennal lobe (AL), but we used two copies to allow imaging at low laser intensities. We imaged neural activity in an identified glomerulus, DM2 (**Fig. 5a**) in response to the presentation of two odours, vinegar and isoamyl acetate. We found a ~4-fold increased fluorescence change in DM2 for GCaMP3 compared to GCaMP1.6, as measured by frame-scans (**Fig. 5b,c**) in response to vinegar (average $\Delta F/F$ of GCaMP3 is 143.7 ± 16.7%; average $\Delta F/F$ of GCaMP1.6 is 39.3 ± 10.9%). Similar results were obtained with glomerulus DM2 when the fly was stimulated with isoamyl acetate odour (data not shown). These data show that GCaMP3 is a major improvement over existing GCaMPs for measuring sensory-evoked Ca^{2+} transients in invertebrates.

Imaging evoked and spontaneous Ca^{2+} transients in the mouse cortex *in vivo*

We delivered GCaMP3 to layer 2/3 somatosensory or motor cortical neurons *via* infection with adeno-associated virus (AAV2/1; *synapsin-1* promoter). Twelve days after infection, we observed robust expression of GCaMP3 in layer 2/3 pyramidal neurons (**Fig. 1e**). We used two-photon microscopy to image labeled cell bodies while simultaneously recording action potentials in whole-cell or cell-attached configurations (**Fig. 6a**).

We first tested the fluorescence changes of GCaMP3 evoked by action potentials that were triggered by brief current pulses in anesthetized mice. The average fluorescence response of GCaMP3 was nearly linearly related to the number of action potentials in trains of 1, 2, 3, 5 or

10 at 50 Hz (**Fig. 6b,c**). A single AP caused a fluorescence increase of 7.9 ± 2.8% (n = 9 cells) (**Fig. 6c**). For bursts of 2, 3, 5 and 10 AP, the corresponding responses were 12.5 ± 6.4%, 21.2 ± 6.4%, 43.7 ± 18.0% and 94.7 ± 42.5%, respectively (n = 9 cells) (**Fig. 6c**). The detection rate was 70% for single pulses, 90% for trains of 3 AP, and 100% for longer trains (**Supplementary Fig. 8b**). Consistent with rapid calcium extrusion at physiological temperature (37°C) [26], GCaMP3 showed faster kinetics *in vivo* (decay $T_{1/2}$ at 10 pulses: 384 ± 76 ms) compared to slice preparations (p = 0.0015, paired t-test).

We next imaged the fluorescence changes of GCaMP3 in response to sensory-evoked and spontaneous calcium transients in the primary motor cortex of awake mice running on a treadmill while recording action potentials in a loose seal cell-attached configuration (**Fig. 6d**). The fluorescence change of GCaMP3 was linearly correlated with the number of action potentials from 3 APs up to 20 APs per 0.5 s (n = 6 cells from 3 animals) (**Fig. 6e**). Single and double action potentials were not reliably detected, likely due to movement noise and elevated baseline calcium levels in the awake brain.

Chronic imaging with GCaMP3 in mice

Long-term expression of GECIs in cortical neurons introduced *via in utero* electroporation caused altered physiology in some cells. We found that ~8.3% of GCaMP3-, 13% of D3cpV- and 5% of TN-XXL- labeled L2/3 pyramidal neurons showed bright nuclear fluorescence at P25-P28 (**Supplementary Fig. 11a**). Neurons with filled nuclei had attenuated GCaMP fluorescence responses (data not shown), and reduced calcium changes evoked by neural activity (**Supplementary Fig. 11b**). Anti-His_6 immuno-staining detected predominantly cytosolic GCaMP3, suggesting that the nuclei are filled with N-terminally cleaved GCaMP3

(**Supplementary Fig. 11c**). These results suggest that both calcium homeostasis and GECI function are impaired in neurons with labeled nuclei.

When GCaMP3 was introduced post-natally *via* viral transduction (under the control of the *synapsin-1* promoter), some neurons near the injection site were bright and nuclear-filled (**Supplementary Fig. 11d**). The spontaneous fluorescence transients of nuclear-filled neurons had long decay times, another signature of abnormal physiology (**Fig. 6f**). These perturbed cells were easily visually identified for exclusion. Basal fluorescence decreased with distance from the injection site and was nuclear-excluded over large areas of the brain, even after 120 days of expression (**Fig. 6f and Supplementary Fig. 11d**). We used a variety of physiological methods to test for altered properties of nuclear-excluded, GCaMP3-positive neurons. We recorded in brain slices from neurons expressing GCaMP3 for 2-3 weeks. GCaMP3-positive neurons had similar resting potential and excitability compared to GCaMP3-negative cells (**Supplementary Fig. 12a,b**). We used laser scanning photostimulation circuit mapping [27] to test for changes in synaptic properties of GCaMP3-positive neurons. We found that GCaMP3-positive and GCaMP3-negative neurons had indistinguishable total synaptic input (**Supplementary Fig. 12c,d**). Thus, broad swathes of cortical surface expressed G-CaMP3 at levels suitable for quantitative optical physiology.

We used GCaMP3 to image the *in vivo* calcium activity of motor cortical neurons repeatedly through a cranial window (**Fig. 6g**). Numerous neurons displayed large-amplitude fluorescence transients during a 140 s imaging period while head-fixed mice ran on a treadmill [28] (**Fig. 6g and Supplementary Movie 3**). Population activity in the motor cortex was correlated with locomotor activity (**Fig. 6g**). The fluorescence decay rates of spontaneous calcium transients in imaged cells with nuclear exclusion were stable 120 days post-infection (**Fig. 6f**).

Repeated imaging of the same neuronal population at 72 and 120 days post-infection showed remarkably constant GCaMP3 expression and signal change (**Fig. 6h**). These results demonstrate that GCaMP3 is suitable for long-term imaging of behaviorally correlated activity in large neuronal populations over extended periods of time.

DISCUSSION

The improved properties of GCaMP3 allow new types of neuroscience applications in multiple model organisms. In *C. elegans*, expression of GECIs has caused behavioral phenotypes [29], likely due to altered neural physiology caused by indicator over-expression (**Supplementary Fig. 10 and Supplementary Table 3**). Neurons expressing GCaMP3 showed high SNR without detectable cytotoxicity or behavioral perturbations (**Supplementary Fig. 10**). The much higher signal levels provided by GCaMP3 (**Fig. 4**) may allow experiments with lower expression levels, ameliorating problems associated with calcium buffering.

In *Drosophila*, the poor expression of GCaMP2 [25] has left GCaMP1.3 and 1.6 as the state-of-the-art single-FP indicators. Their poor sensitivity and non-linear response has precluded detection of low firing rates [30]. GCaMP3 showed greatly improved expression and signal levels *in vivo* (**Fig. 5**) with no apparent cytotoxicity or behavioral phenotype (data not shown), and could permit imaging experiments not previously possible.

In behaving mice, GCaMP3 allows the simultaneous recording of the activity of dozens of identified neurons over months (**Fig. 6g,h**). Thus, GCaMP3 should allow tracking learning-induced changes in circuit-level activity over multiple recording sessions. Pan-neuronal expression of GCaMP3 might allow wide-field imaging of whole-cortex activity and signal propagation akin to super-resolution functional MRI [31].

Long-term, high-level expression of GECIs in the mouse brain can result in non-functional indicators[32] and abnormal physiology (**Supplementary Fig. 11**). Though expression of GCaMP3 in the postnatal brain, mediated by viral gene transfer, limited such adverse effects, the proportion of nuclear-filled neurons still increased with proximity to the injection site, and

slowly increased with time after injection. Therefore, optimizing the timing and magnitude of expression to balance signal levels and cytotoxicity needs further study.

Ratiometric indicators have potential advantages over single-FP GECIs, including higher baseline brightness and insensitivity to motion artifacts *via* wavelength ratioing. However, GCaMP3 is more photostable, likely because of reduced bleaching in the low fluorescence state (**Fig. 3g**). Ratiometric measurements could be achieved with GCaMP3 by co-expression or fusion of a reference fluorescent protein. The smaller size of GCaMP3 potentially facilitates a wider array of targeted protein fusions for calcium imaging in subcellular compartments. The faster kinetics of GCaMP3 may allow more faithful detection of the number and timing of action potentials in spike trains.

GCaMP3 may not be the most suitable GECI for all applications. Single action potentials can also be detected using D3cpV [14]; indeed, the slow kinetics of D3cpV might be suitable for situations characterized by very low and sparse spike rates. Troponin-based indicators, such as TN-XXL, may cause less perturbation of endogenous calcium signaling [6]. Prudence dictates testing each of these indicators in the context of specific applications.

Although GCaMP3 is a major improvement over GCaMP2, additional avenues for protein engineering remain. Quantitative modeling studies [20] have suggested that increasing the fluorescence on-rate would further improve detection of the brief calcium transients associated with single APs. Expression cassettes that maintain steady, moderate levels of GCaMP3 expression for months would facilitate signal calibration and further reduce toxicity concerns.

Acknowledgements
We would like to thank J. Simpson and S. Hampel for cloning GCaMPs into pMUH, and the Fly Core for making fly crosses. pMUH was a generous gift from B. Pfeiffer and G. Rubin. Thanks to J. Seelig who contributed to the *Drosophila* imaging experiments. Thanks to S. Viswanathan and S. Sternson for assistance in screening mutants in HEK293 cells, and J. Marvin for assistance in screening mutants in *E. coli*. Thanks to B. Zemelman for assistance in virus production. Thanks to H. Zhong, T. Sato and B. Borghuis for developing image analysis software. Thanks to D. K. O'Connor for *in utero* electroporation assistance. Thanks to H. White and S. Winfrey for cell culture, B. Shields and A. Hu for histology, and A. Arnold for imaging experiments. Thanks to the Molecular Biology Shared Resource for plasmid preparation and sequencing. Thanks to J. Marvin, J. Simpson and G. Tervo for critical reading of the manuscript. All affiliations are Howard Hughes Medical Institute, Janelia Farm Research Campus.

Author contributions
L.L.L., K.S., L.T., S.A.H., T.M., design of project; L.T., L.L.L., sensor design and screen in *E. coli*, HEK293 cells; L.T., T.M., S.A.H., L.P., GCaMP variant testing in brain slice; S.A.H., FRET sensor and GCaMP2 testing in brain slice; S.A.H., L.T., D.H., imaging data analysis of brain slice and *in vivo*; D.H., *in vivo* mouse brain imaging; S.C., C.B., worm imaging and data analysis; V.J., E.C., calcium imaging and data analysis in fly; S.A.M, S.A.H., data analysis for AP detection probability; J.A.,L.L.L, E.R.S., structure analysis; L.L.L. and L.T., led the project; L.L.L., K.S., L.T. and S.A.H., wrote the paper.

Competing interests statement
The authors declare no competing financial interests.

REFERENCES

1. Yuste, R., Peinado, A. & Katz, L. C. Neuronal domains in developing neocortex. *Science* **257**, 665-669 (1992).
2. Stosiek, C., Garaschuk, O., Holthoff, K. & Konnerth, A. In vivo two-photon calcium imaging of neuronal networks. *Proc Natl Acad Sci U S A* **100**, 7319-7324 (2003).
3. Fetcho, J. R., Cox, K. J. & O'Malley, D. M. Monitoring activity in neuronal populations with single-cell resolution in a behaving vertebrate. *Histochem J* **30**, 153-167 (1998).
4. Tour, O. et al. Calcium Green FlAsH as a genetically targeted small-molecule calcium indicator. *Nat Chem Biol* **3**, 423-431 (2007).
5. Palmer, A. E. & Tsien, R. Y. Measuring calcium signaling using genetically targetable fluorescent indicators. *Nat Protoc* **1**, 1057-1065 (2006).
6. Mank, M. et al. A genetically encoded calcium indicator for chronic in vivo two-photon imaging. *Nat Methods* (2008).
7. McCombs, J. E. & Palmer, A. E. Measuring calcium dynamics in living cells with genetically encodable calcium indicators. *Methods* **46**, 152-159 (2008).
8. Mank, M. & Griesbeck, O. Genetically encoded calcium indicators. *Chem Rev* **108**, 1550-1564 (2008).
9. Baird, G. S., Zacharias, D. A. & Tsien, R. Y. Circular permutation and receptor insertion within green fluorescent proteins. *Proc Natl Acad Sci U S A* **96**, 11241-11246 (1999).
10. Nagai, T., Sawano, A., Park, E. S. & Miyawaki, A. Circularly permuted green fluorescent proteins engineered to sense Ca2+. *Proc Natl Acad Sci U S A* **98**, 3197-3202 (2001).
11. Miyawaki, A. et al. Fluorescent indicators for Ca2+ based on green fluorescent proteins and calmodulin. *Nature* **388**, 882-887 (1997).

12. Heim, N. & Griesbeck, O. Genetically encoded indicators of cellular calcium dynamics based on troponin C and green fluorescent protein. *J Biol Chem* **279**, 14280-14286 (2004).
13. Palmer, A. E. et al. Ca2+ indicators based on computationally redesigned calmodulin-peptide pairs. *Chem Biol* **13**, 521-530 (2006).
14. Wallace, D. J. et al. Single-spike detection in vitro and in vivo with a genetic Ca(2+) sensor. *Nat Methods* (2008).
15. He, J., Ma, L., Kim, S., Nakai, J. & Yu, C. R. Encoding gender and individual information in the mouse vomeronasal organ. *Science* **320**, 535-538 (2008).
16. Chalasani, S. H. et al. Dissecting a circuit for olfactory behaviour in Caenorhabditis elegans. *Nature* **450**, 63-70 (2007).
17. Wang, J. W., Wong, A. M., Flores, J., Vosshall, L. B. & Axel, R. Two-photon calcium imaging reveals an odor-evoked map of activity in the fly brain. *Cell* **112**, 271-282 (2003).
18. Akerboom, J. et al. Crystal structures of the GCaMP calcium sensor reveal the mechanism of fluorescence signal change and aid rational design. *J Biol Chem* (2008).
19. Wang, Q., Shui, B., Kotlikoff, M. I. & Sondermann, H. Structural Basis for Calcium Sensing by GCaMP2. *Structure* **16**, 1817-1827 (2008).
20. Hires, S. A., Tian, L. & Looger, L. L. Reporting neural activity with genetically encoded calcium indicators. *Brain Cell Biol* **36**, 69-86 (2008).
21. Varshavsky, A. The N-end rule at atomic resolution. *Nat Struct Mol Biol* **15**, 1238-1240 (2008).
22. Pedelacq, J. D., Cabantous, S., Tran, T., Terwilliger, T. C. & Waldo, G. S. Engineering and characterization of a superfolder green fluorescent protein. *Nat Biotechnol* **24**, 79-88 (2006).

23. Pologruto, T. A., Yasuda, R. & Svoboda, K. Monitoring neural activity and [Ca2+] with genetically encoded Ca2+ indicators. *J Neurosci* **24**, 9572-9579 (2004).

24. Mao, T., O'Connor, D. H., Scheuss, V., Nakai, J. & Svoboda, K. Characterization and subcellular targeting of GCaMP-type genetically-encoded calcium indicators. *PLoS ONE* **3**, e1796 (2008).

25. Hendel, T. et al. Fluorescence changes of genetic calcium indicators and OGB-1 correlated with neural activity and calcium in vivo and in vitro. *J Neurosci* **28**, 7399-7411 (2008).

26. Markram, H., Helm, P. J. & Sakmann, B. Dendritic calcium transients evoked by single back-propagating action potentials in rat neocortical pyramidal neurons. *J Physiol* **485**, 1-20 (1995).

27. Shepherd, G. M. & Svoboda, K. Laminar and columnar organization of ascending excitatory projections to layer 2/3 pyramidal neurons in rat barrel cortex. *J Neurosci* **25**, 5670-5679 (2005).

28. Dombeck, D. A., Khabbaz, A. N., Collman, F., Adelman, T. L. & Tank, D. W. Imaging large-scale neural activity with cellular resolution in awake, mobile mice. *Neuron* **56**, 43-57 (2007).

29. Ferkey, D. M. et al. C. elegans G protein regulator RGS-3 controls sensitivity to sensory stimuli. *Neuron* **53**, 39-52 (2007).

30. Jayaraman, V. & Laurent, G. Evaluating a genetically encoded optical sensor of neural activity using electrophysiology in intact adult fruit flies. *Front Neural Circuits* **1**, 3 (2007).

31. Kim, S. G. & Ogawa, S. Insights into new techniques for high resolution functional MRI. *Curr Opin Neurobiol* **12**, 607-615 (2002).

32. Hasan, M. T. et al. Functional fluorescent Ca2+ indicator proteins in transgenic mice under TET control. *PLoS Biol* **2**, e163 (2004).

FIGURE LEGENDS

Figure 1. *In vitro* characterization of GCaMP3. (**a**) Screening resulted in several mutants with improved baseline brightness and signal change in HEK293 cells. (**b**) Schematic representation of GCaMP2 and GCaMP3. Mutated residues are highlighted in red. (**c**) Fluorescence spectra of GCaMP3 and GCaMP2 (1 μM protein) with 1 mM Ca^{2+} or 10 mM EGTA in MOPS buffer (30 mM MOPS, 100 mM KCl, pH 7.5) (average of three independent measurements). The fluorescence intensity of each indicator was normalized to the peak of the calcium-saturated spectrum. The inset shows the un-normalized fluorescence emission spectra (485 nm excitation). (**d**) Ca^{2+} titration curve (1 μM protein) in MOPS buffer. Inset shows the dynamic range of the two indicators. (**e**) The improved baseline fluorescence of GCaMP3 compared to GCaMP2. Both indicators were either transfected to HEK293 cells or virally delivered to layer 2/3 cortical neurons. Images were taken either 48 hours post-transfection or 12 days post-viral injection, then analyzed with Volocity5.0 (Improvision). 50 μm scale bar. Error bars indicate standard deviation of the mean.

Figure 2. Action potential-evoked response of GCaMP3 in hippocampal pyramidal and layer 2/3 cortical neurons. (**a**) Linescan location at the base of the apical dendrite and evoked action potentials in the soma. 10 μm scale bar. Raw linescan images showing fluorescence baseline and single action potential-evoked responses. (**b**) Average-trial responses of GCaMP3 for individual hippocampal pyramidal cells in organotypic slices (n = 9 cells, thin gray lines) and mean across all cells (thick black line) for each stimulus. Note different y-axis scales for each panel. (**c**) Expression of GCaMP3 in layer 2/3 cortical neurons (S1) *via in utero* electroporation.

20 μm scale bar. (**d**) Average-trial responses of GCaMP3 for individual layer 2/3 cortical cells (n = 9 cells, thin gray lines) in response to trains of action potentials given at 83 Hz, and the mean across cells (thick black line). Note different y-axis scales for each panel. (**e, f**) Amplitudes and SNR of GCaMP3 responses for individual hippocampal pyramidal cells (thin gray lines) in response to trains of action potentials given at 83 Hz, and the mean across cells (thick red line). (**g**) The average response of GCaMP3 is greater than GCaMP2. (**h**) The SNR of GCaMP3 is also greater than GCaMP2. Error bars indicate standard deviation of the mean.

Figure 3. Comparison of GECI responses in pyramidal cell principal dendrite in acute cortical slice to back-propagating action potentials. (**a**) Schematic representation of the FRET-based calcium indicators D3cpV and TN-XXL. (**b**) Mean of fluorescence responses for action potential trains across cells (n = 7 cells, 1 trial each cell). Traces from bottom to top represent the response to trains of 1, 2, 3, 5, 10, 20 and 40 APs. (**c**) Ratio change of D3cpV and TN-XXL for individual hippocampal pyramidal cells (thin gray lines) in response to trains of action potentials given at 83 Hz, and the mean across cells (thick black line). (**d**) SNR of D3cpV and TN-XXL. (**e, f**) Comparison of mean responses ($\Delta F/F$ or $\Delta R/R$) and SNR of GCaMP3, D3cpV and TN-XXL. Zoom of lower stimuli is shown in inset. (**g**) Mean cellular fluorescence during periodic two-photon frame scans (n = 3-4 cells per GECI). (**h**) Rise and decay time comparison of all three indicators at 10 APs. Error bars indicate standard deviation of the mean.

Figure 4. *In vivo* imaging of sensory-evoked Ca^{2+} transients with GCaMPs in *C. elegans.* Odour-evoked responses of GCaMP1, GCaMP2 and GCaMP3 in *C. elegans* olfactory neurons. Transgenic worm lines expressing GCaMPs were imaged following an odour addition-removal sequence. (**a,b**) Upon odour presentation, GCaMP3 and GCaMP2 showed a similar decrease in fluorescence intensity. (**c,d**) Upon odour removal, GCaMP3 showed a 4- to 5-fold increase of fluorescence response compared to GCaMP2 and GCaMP1. Grey bars denote odour presence. Yellow intervals were analyzed in **b** and **d**. Shading of each trace and error bars indicate standard error of the mean (S.E.M., n = 12 animals for each genotype).

Figure 5. *In vivo* imaging of sensory-evoked Ca^{2+} transients with GCaMPs in *Drosophila*. Odour-evoked responses of GCaMP1.6 and GCaMP3 in projection neurons of the *Drosophila* antennal lobe (AL). (**a**) Expression of GCaMP1.6 and GCaMP3 in DM2 glomeruli of the AL. DM2 ROI, circled with dashed line, was used for framescans. 10 μm scale bar. (**b**) Comparison of DM2 framescan responses of GCaMP1.6 and GCaMP3 to presentations of vinegar. 5-trial average response of a single animal each, expressing GCaMP1.6 (left panel) or GCaMP3 (right panel). (**c**) Peak response of GCaMP1.6 (4ALs from 3 animals) and GCaMP3 (4ALs from 4 animals) across all trials and animals. The response of GCaMP3 was increased ~4-fold compared to GCaMP1.6. Comparisons shown here are significant (p = 6.80e-08, Mann-Whitney). Error bars indicate standard deviation of the mean.

Figure 6. ***In vivo*** **Ca^{2+} imaging of evoked and spontaneous activity with GCaMP3 in awake, behaving mice.** (**a**) Schematic illustrating simultaneous two-photon imaging and electrophysiology in virally infected L2/3 neurons *in vivo*. (**b**) Examples of single-trial responses (gray line) and average across 10 trials (black line) from three neurons to evoked APs at 50 Hz under anesthesia. (**c**) GCaMP3 showed linear ΔF/F in response to evoked APs (n = 9 cells, thin gray lines; average of 10 trials per neuron, thick red line). (**d**) Example trace of simultaneous recording of fluorescence changes (black) and spiking activity (red, number of APs per 0.5 sec bin) during head-fixed behavior. APs were recorded in loose seal cell-attached mode. (**e**) Fluorescence change in response to action potentials, binned over 0.5 s intervals. 6 cells from 3 animals were indicated with different colors. Error bars indicate standard deviation of the mean. (**f**) Cumulative distribution of the decay times ($T_{½}$, single-exponential fit from last fluorescence maximum). Decay times of neurons with nuclear exclusion are similar at 10 to 120 days (colored lines, p = 0.22, Kolmogorov–Smirnov test). Nuclear-filled neurons have significantly longer decay times (black line, p = 5.78e-10, Kolmogorov–Smirnov test). (**g**) GCaMP3 expression in L2/3 neurons of the primary motor cortex at 72 days post injection (top, 30 μm scale bar) and ΔF/F traces of individual cells (bottom, black lines). Relative treadmill movement indicated by red line (F: forward, B: backward). (**h**) The same field of view and fluorescent traces as (g) at 120 days post injection.

Supplementary File	Title
Supplementary Figure 1	Improving the protein stability of GCaMP2.
Supplementary Figure 2	Summary of positions where mutants were generated
Supplementary Figure 3	Screening of GCaMP2 mutants in a HEK293 cell based assay.
Supplementary Figure 4	Screening resulted in several mutants with improved baseline brightness and signal change in HEK 293 cells.
Supplementary Figure 5	Examples of single-trial responses of GCaMP3
Supplementary Figure 6	Imaging spontaneous activity of neurons in hippocampal slice using GCaMP2 and GCaMP3
Supplementary Figure 7	Examples of single-trial fluorescence responses of GCaMP3 to low frequency stimuli
Supplementary Figure 8	Examples of single-trial responses of D3cpV (top panel) or TN-XXL
Supplementary Figure 9	Action potential detection probability
Supplementary Figure 10	Expressing GECIs in *C.elegans*
Supplementary Figure 11	Long-term expression of GECIs can cause altered neuron morphology and sensor properties
Supplementary Figure 12	Intrinsic and circuit properties of neurons with or without expression of GCaMP3
Supplementary Table 1	Summary of the improved GCaMPs from HEK 293 cell-based screening
Supplementary Table 2	Comparing GCaMP3 with GCaMP2 and the FRET-based sensors
Supplementary Table 3	Expression of Genetically-encoded calcium indicators in AWC neurons of *C. elegans*
Supplementary Video 1	Spontaneous neural activity visualized by GCaMP2 in cultured hippocampal brain slice (3x realtime)
Supplementary Video 2	Spontaneous neural activity visualized by GCaMP3 in cultured hippocampal brain slice (3x realtime)
Supplementary Video 3	Naturally occurring activity of populations of layer 2/3 neurons expressing GCaMP3 in the primary motor cortex (M1) of awake, behaving mouse during 140 sec sequence of two•photon images (10X real time)

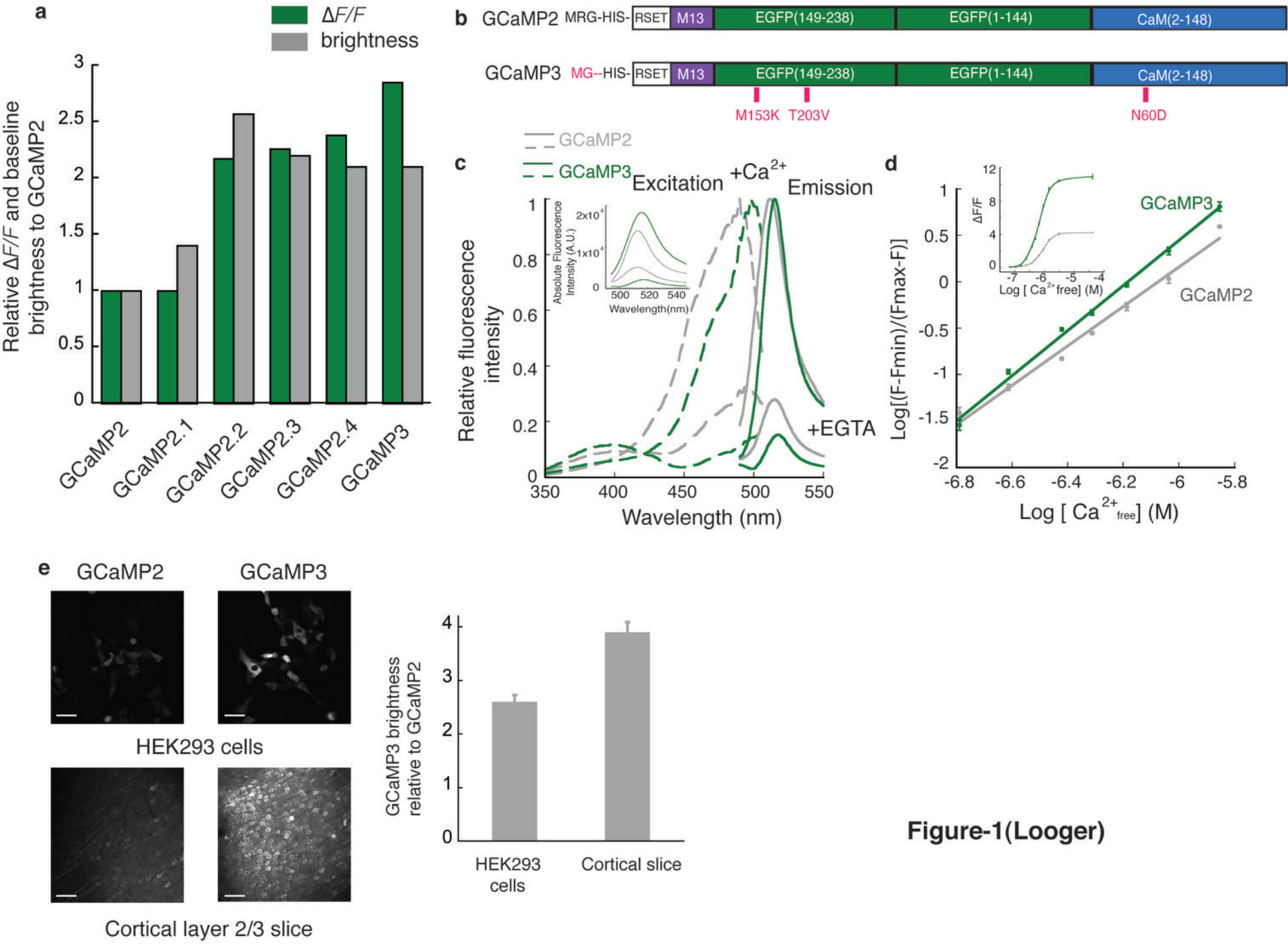

Figure-1(Looger)

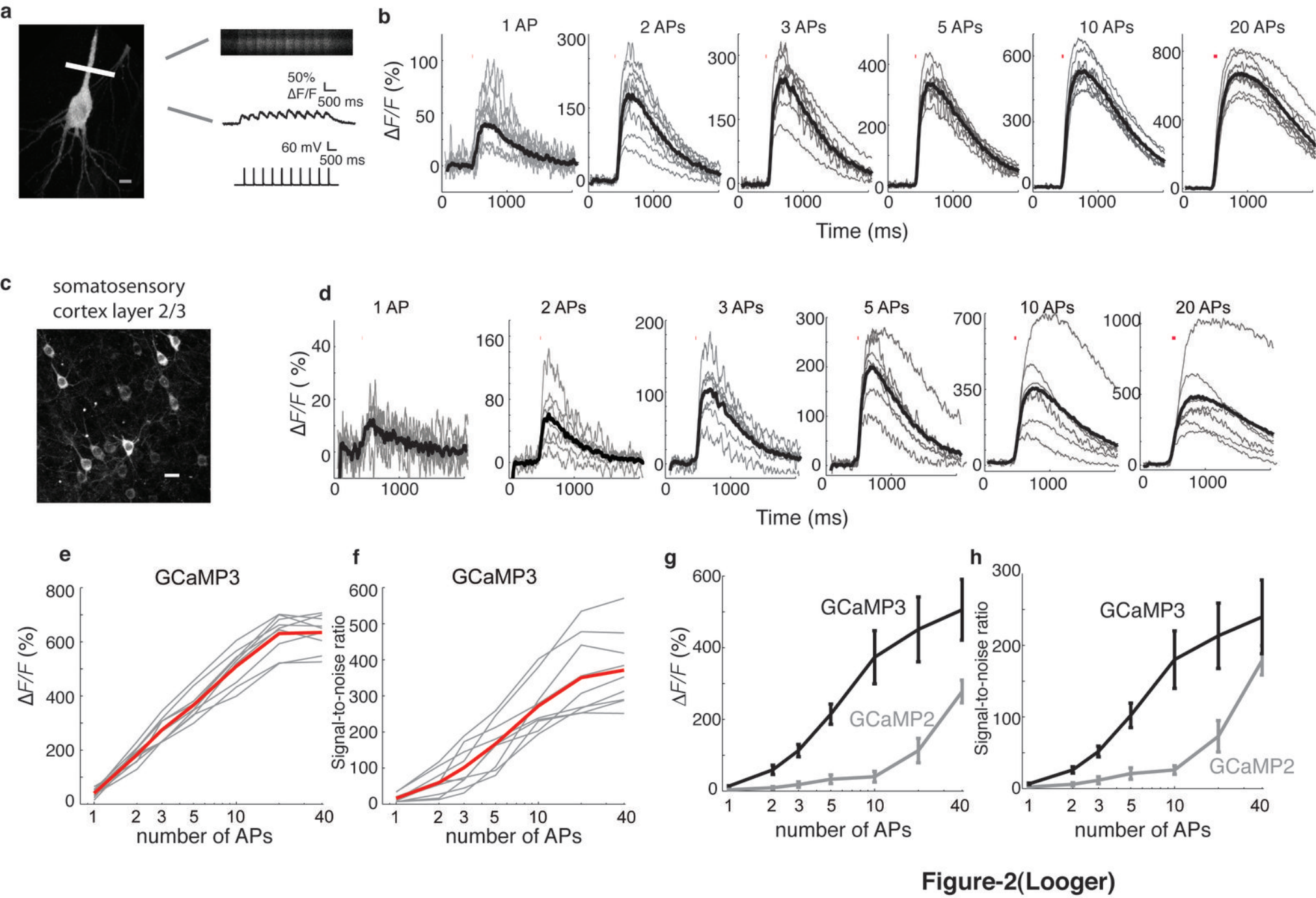

Figure-2(Looger)

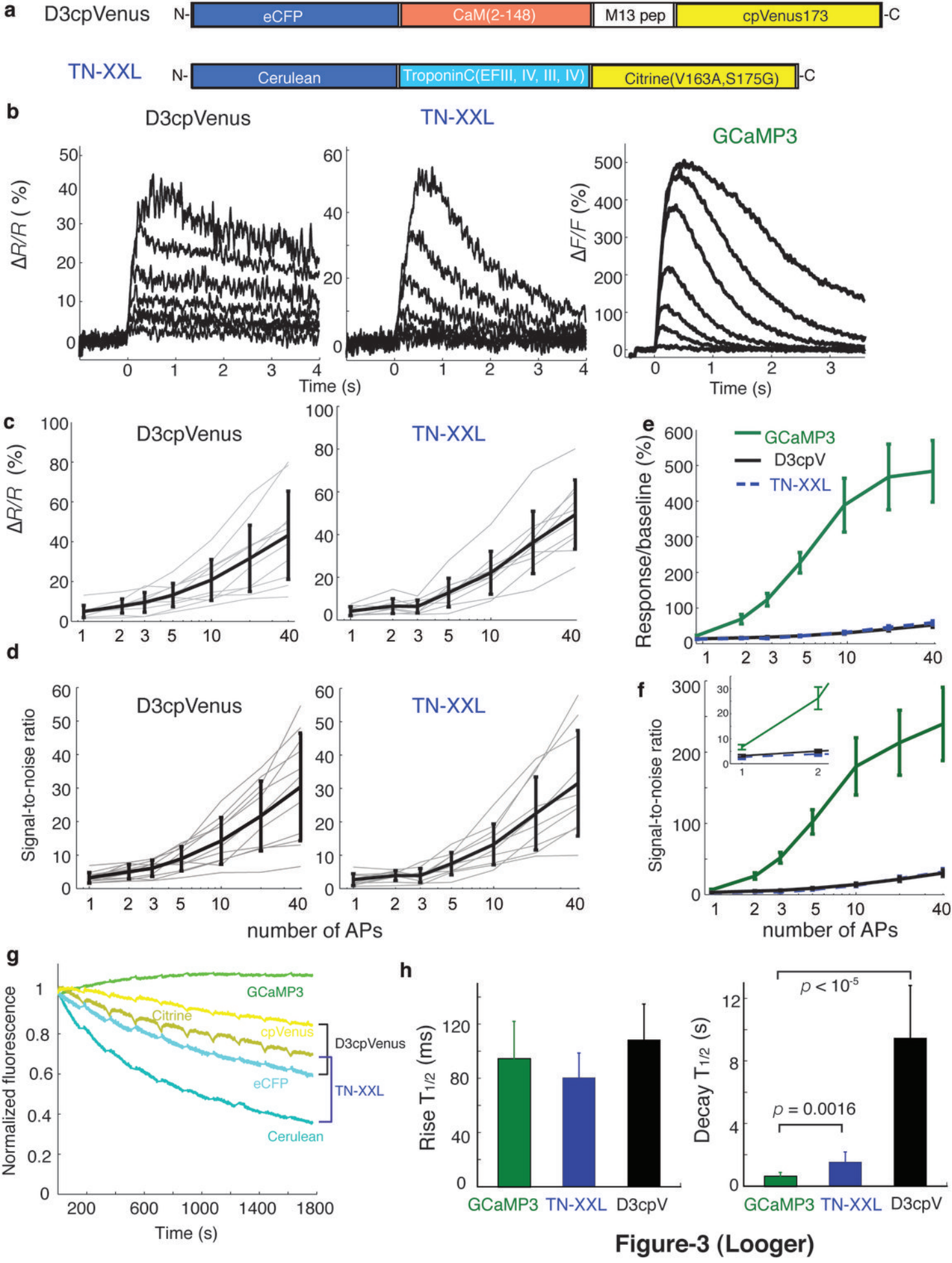

Figure-3 (Looger)

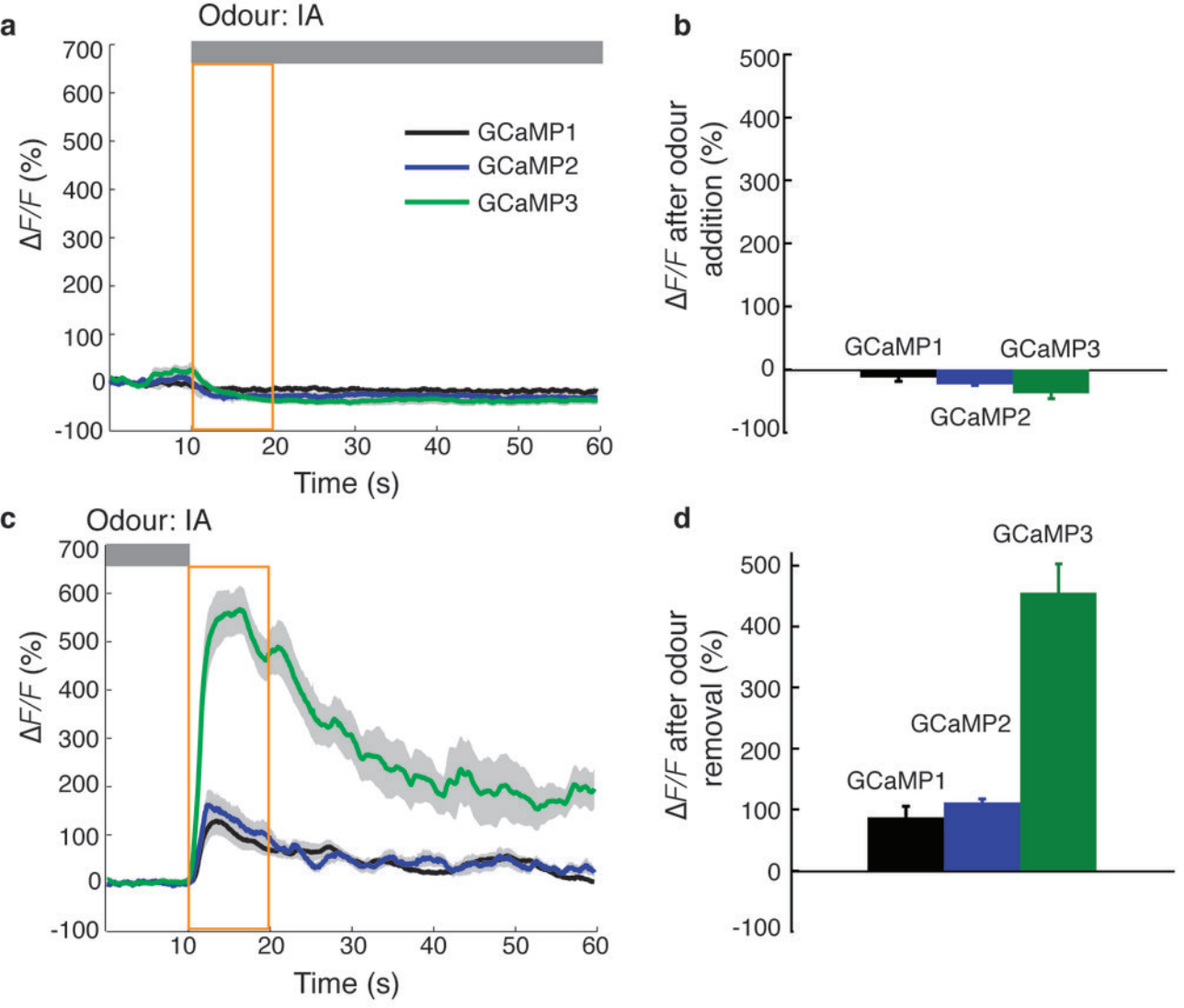

Figure-4 (Looger)

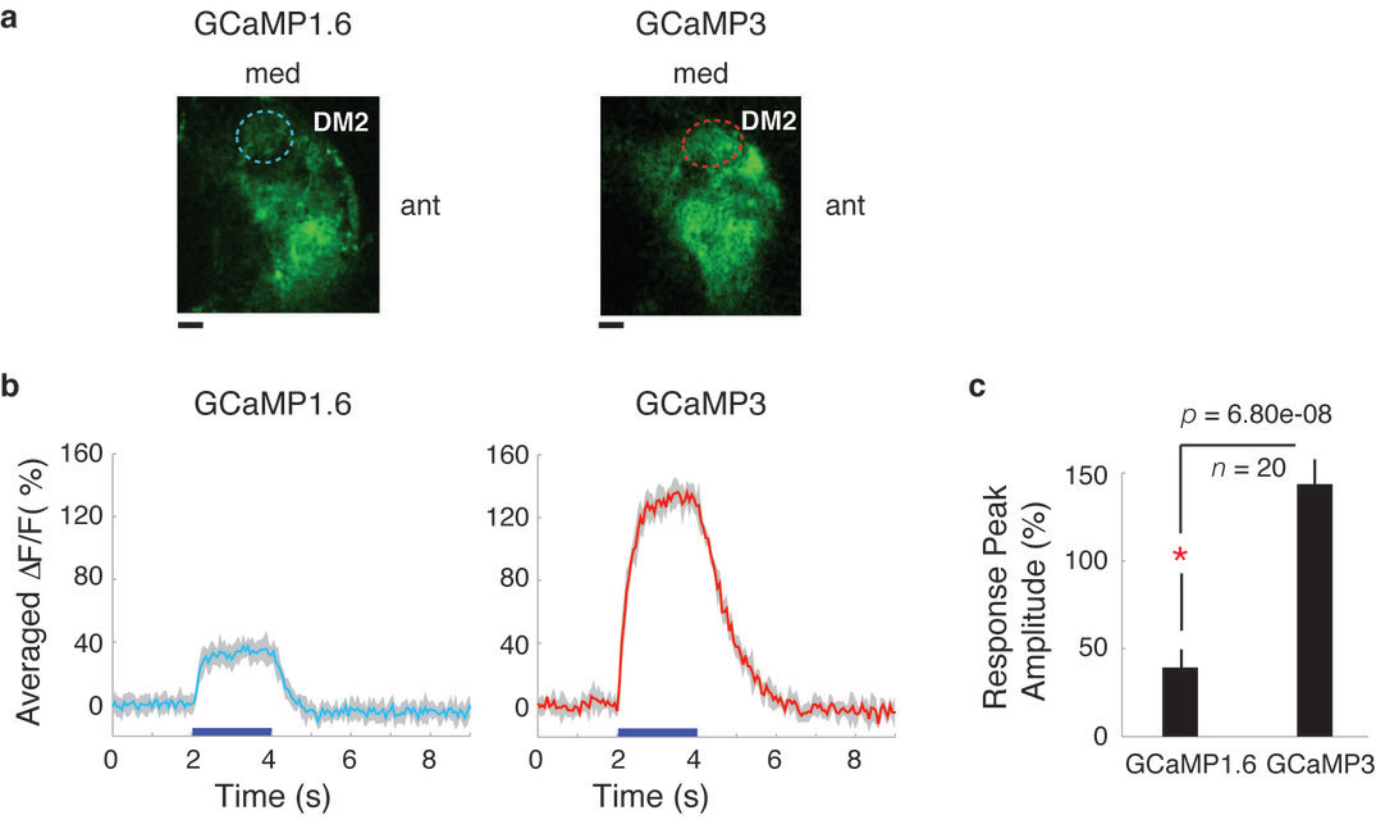

Figure-5 (Looger)

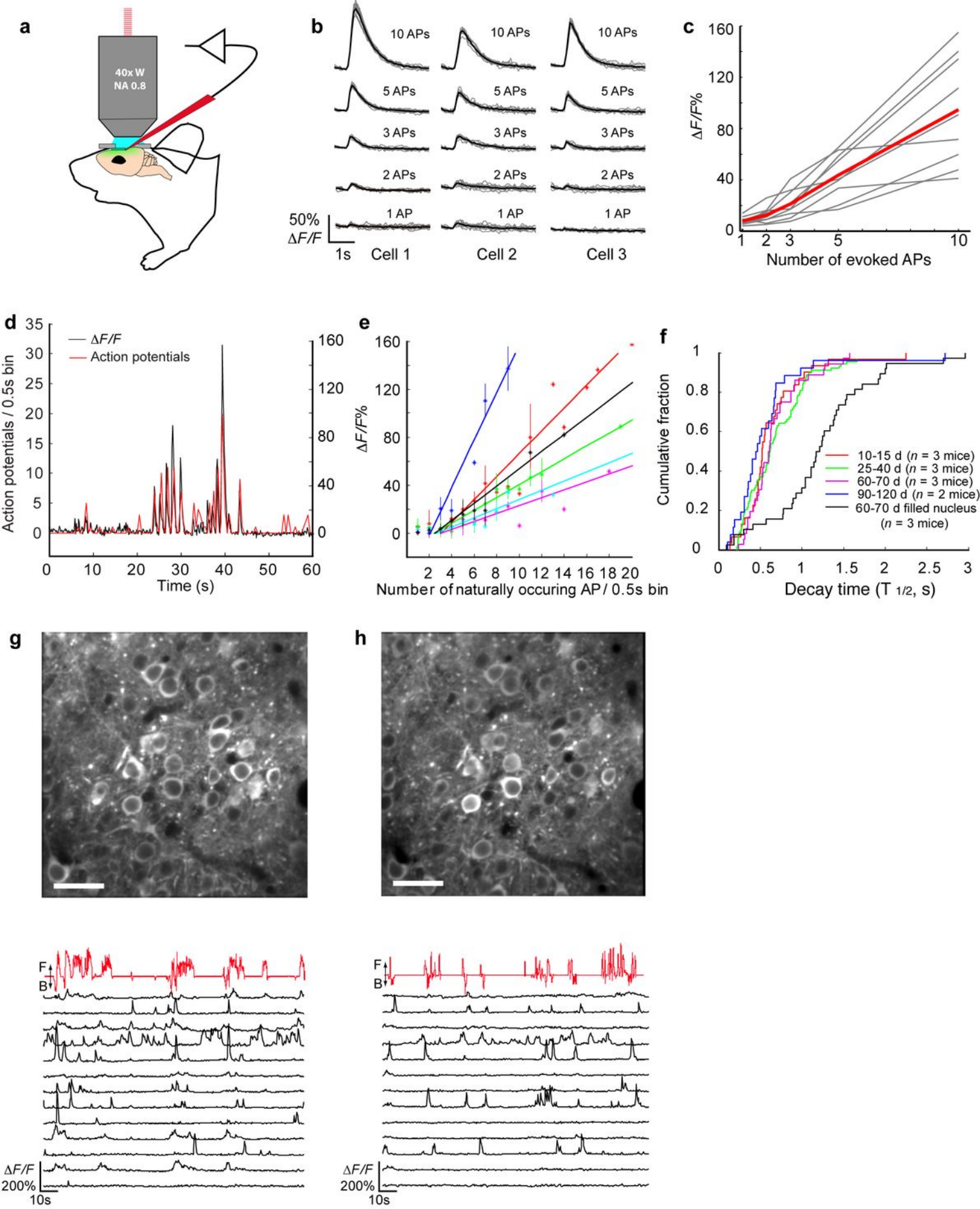
a
40x W
NA 0.8
b
10 APs
5 APs
3 APs
2 APs
1 AP
50%
ΔF/F
1s
Cell 1
Cell 2
Cell 3
c
ΔF/F%
Number of evoked APs
d
ΔF/F
Action potentials
Action potentials / 0.5s bin
Time (s)
e
ΔF/F%
Number of naturally occuring AP / 0.5s bin
f
Cumulative fraction
10-15 d (n = 3 mice)
25-40 d (n = 3 mice)
60-70 d (n = 3 mice)
90-120 d (n = 2 mice)
60-70 d filled nucleus
(n = 3 mice)
Decay time (T 1/2, s)
g
h
F
B
ΔF/F
200%
10s